# Geometry of the Pentachlorocuprate(II) Ion

**Georgi St. Nikolov**

Department of Physical and Theoretical Chemistry, University of Plovdiv, Plovdiv 4000, Bulgaria, and Institute of General and Inorganic Chemistry, Bulgarian Academy of Sciences, Sofia 1113, Bulgaria

*Received March 9, 1993*[⊗]

The geometry of the $[CuCl_5]^{3-}$ unit was studied by the Extended Huckel Method with distance-dependent off-diagonal elements in an attempt to explain why the unit exists at >280 K as a compressed trigonal bipyramid (TBP) with symmetry $D_{3h}$ and at <280 K as an elongated pyramid with symmetry $C_{2v}$. Three routes for $D_{3h}$–$C_{2v}$ interconversion were considered: Berry pseudorotation exchanging the TBP axial and equatorial ligands without (path 1) or with (path 2) equatorial bond stretching, where one bond is pivotal in this process; bending and stretching only in the equatorial plane with the two axial bonds being pivotal (path 3). The three paths are governed by the TBP's totally symmetric $2\alpha_1'$ and degenerate $3\epsilon'$ vibrational modes taken in different combinations. The global energy minimum as a function of the TBP vibrational coordinates occurs for the $C_{2v}$ symmetry. The compressed TBP structure ($D_{3h}$) is a local minimum readily accessible from the $C_{2v}$ structure at >280 K. Route 3 with fixed axial bonds dominates the interconversion process. The two totally symmetric modes $\alpha_1'$ play a very important role in this process since they compress the TBP and facilitate the equatorial bond changes.

## 1. Introduction

The $[CuCl_5]^{3-}$ unit exists in various compounds with different counterions.[1-7] The counterion seems to contribute slightly to shaping the $[CuCl_5]^{3-}$ geometry. The most remarkable feature of the compounds involving $[CuCl_5]^{3-}$ units is a crystal phase transition at temperatures close to 280 K which is accompanied by changes in the $[CuCl_5]^{3-}$ geometry. There are two recorded and comparatively well-documented cases of such transitions:

(a) In $[Cr(NH_3)_6][CuCl_5]$ at room temperature, $[CuCl_5]^{3-}$ is a compressed trigonal bipyramid (TBP) ($R_{eq}$ = 2.3912 Å; $R_{ax}$ = 2.2964 Å).[2,3] On the basis of unresolved unpolarized reflectance spectra, it is supposed[1,8] that at temperatures lower than 280 K the TBP is converted to an elongated square pyramid (SP) with $C_{4v}$ symmetry. However a low-temperature X-ray determined structure is lacking, and the available spectral data may be better interpreted in terms of a lower symmetry, possibly $C_{2v}$.

(b) The $[Co(CH_3)_6][CuCl_5]$ compound[7] is cubic $Fd3c$ ($O_h^8$); at 299 K the $CuCl_5$ unit is a compressed TBP (see Figure 1). At 120 K the phase is tetragonal $I4_1/adc$ ($D_{4h}^{20}$) and the $CuCl_5$ unit is an elongated pyramid with $C_{2v}$ symmetry.[7] The $C_{2v}$ structure can alternatively be described as a TBP with unequal equatorial bonds. The crystal phase transition occurs at 280.8 K.

The Jahn–Teller cooperative coupling[9] should be ruled out in these phase transitions since no order–disorder is detected in the crystal state. To explain the indicated phase transitions and the accompanying change in $[CuCl_5]^{3-}$ geometry, pseudo-Jahn–Teller local coupling was invoked.[10-13]

Electronic structure calculations on $[CuCl_5]^{3-}$ with different methods[10-13] have shown that the pyramidal $C_{2v}$ structure is more stable than the bipyramidal $D_{3h}$ one. For this reason, its appearance in the low-temperature phase is not surprising. In some 5-coordinate Cu(II) complexes with organic ligands, external high pressure induces changes from TBP to a more symmetric pyramidal structure.[14]

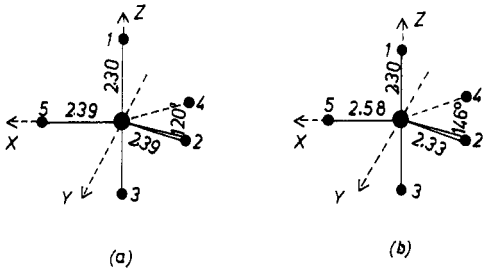


**Figure 1.** $[CuCl_5]^{3-}$ unit in $[Co(NH_3)_6][CuCl_5]$[7] at 299 K (a) and at 120 K (b). The numbering of the atoms and the orientation of the Cartesian coordinates centered at Cu and used in this work are also given.

On the basis of pseudo-JT coupling (PJTC) treated in the angular overlap model (AOM) formalism, the TBP structure was supposed[1,11] to be a thermal average of differently oriented square pyramids (SP) with $C_{4v}$ symmetry. PJTC in $CuCl_5^{3-}$ has also been employed with the conventional extended Huckel (EH) method.[12] EH and AOM however differ widely over the origin of the PJTC: AOM predicts mixing of the ground state with the first excited state, which is assumed to be a Cu d-AO, while EH suggests a multilevel PJTC in which even remote MOs giving rise to charge transfer excitations contribute to the stabilization. In general the AOM is not suitable to solving PJTC[12] because the intervening MOs are not pure metal ion d AOs.

Recent studies[7] on the crystal and molecular structure of the two temperature phases of $[Co(NH_3)_6][CuCl_5]$ reject the dynamic

[⊗] Abstract published in *Advance ACS Abstracts,* February 1, 1994.

(1) Reinen, D.; Friebel, C. *Inorg. Chem.* **1984**, *23*, 791.
(2) Raymond, K. N.; Meek, D. W.; Ibers, J. A. *Inorg. Chem.* **1968**, *7*, 1111.
(3) Bernal, I.; Korp, J. D.; Schlemper, E. O.; Hussein, M. S. *Polyhedron* **1982**, *1*, 365.
(4) Mori, M.; Saito, Y.; Watanabe, T. *Bull. Chem. Soc. Jpn.* **1961**, *34*, 295.
(5) Wilk, A.; Reinen, D.; Friebel, C. Cited in ref 11.
(6) Duggan, M.; Ray, N.; Hathaway, B. J. *J. Chem. Soc., Dalton Trans.* **1980**, 1342.
(7) Aoyama, T.; Ohba, S.; Saito, Y.; Bernal, I. *Acta Crystallogr.* **1992**, *C48*, 248.
(8) Reinen, D.; Friebel, C. *Struct. Bonding* **1979**, *37*, 1.
(9) Breza, M. *Collec. Czech. Chem. Commun.* **1990**, *55*, 2119. Breza, M. *Acta Crystallogr.* **1990**, *B46*, 573. Boca, R.; Breza, M.; Pelikan, P. *Struct. Bonding* **1989**, *71*, 58.
(10) Bacci, M. *Chem. Phys.* **1986**, *104*, 191; **1987**, *134*, 13.
(11) Reinen, D.; Atanasov, M. A. *Chem. Phys.* **1989**, *136*, 27; **1991**, *155*, 157. Reinen, D. The Jahn-Teller Effect of $Cu^{2+}$ in 6-, 5-, and 4-Coordination. Examples of the Importance of Vibronic Interactions in Transition-Metal Chemistry. In *Vibronic Processes in Inorganic Chemistry*; Flint, C. D., Ed.; Kluwer Academic Publ.: Dodrecht, The Netherlands, p 267.
(12) (a) Bersuker, I. B.; Gorinchoi, N. N.; Polinger, V. Z. *Proceedings of the Tenth International Symposium on the Jahn-Teller Effect*; Moldovian Academy of Sciences Publishing House: Kishinev, Moldova, 1989; p 29; (b) Polinger, V. Z.; Gorinchoi, N. N.; Bersuker, I. B. *Chem. Phys.* **1992**, *159*, 75; (c) Gorinchoi, N. N.; Bersuker, I. B.; Polinger, V. Z. *New J. Chem.* **1993**, *17*, 125.
(13) Langfelderova, H.; Boca, R.; Kozisek, J.; Omelka, L.; Stasko, A. *Proceedings of the Tenth Conference on Coordination Chemistry, Smolenice, Czechoslovakia*; Slovak Technical University, Bratislava, 1985.
(14) Bray, K. L.; Drickamer, H. G. *J. Chem. Phys.* **1989**, *93*, 7604.

0020-1669/94/1333-1144$04.50/0 

PJTC on the basis of the temperature dependence of the thermal parameters for the compressed TBP structure.

We shall examine in this paper the variations of the ground-state energy of the $[CuCl_5]^{3-}$ unit as a function of the reference TBP's vibrational symmetry modes with the purpose of detecting the minima on the ground-state potential energy maps. For practical reasons (the number of computations exceeds several thousand) we shall use a semiempirical method—a new version of the EH method.[15] The conventional EH method produces results of limited absolute values; unlike the conventional EH, however, the new version reflects realistically bond length and valence angle variations.[15] Moreover, our EH calculations refer to the same $CuCl_5$ chromophore but with different stereochemistries, and the results obtained are expected to be relatively correct.

## 2. Theoretical Section

**Extended Huckel Method.** The new EH method in its new iterative version[15] involves calculations of the diagonal elements ($H_{ii}$) from the valence orbital ionization potentials (VOIP) and the orbital populations in the same way as the conventional EH; the off-diagonal elements ($H_{ij}$) are also calculated by the known formula

$$H_{ij} = (1/2)K(H_{ii} + H_{jj})S_{ij} \quad (1)$$

$S_{ij}$ is the overlap integral between the $i$th orbital and the $j$th orbital. The new element is the way the constant $K$ is calculated

$$K = (1 + k)\exp[-\Delta(R - d_0)] \quad (2)$$

where

$$d_0 = r_n(A) + r_n(B) \quad (3)$$

is the sum of orbital radii $r_n$ for atoms A and B, $R$ is the M–L distance, and $\Delta = 0.13$ Å$^{-1}$ and $k = 2.25$ are the optimal values of these constants extracted from EH calculations.[15]

It is evident from (1) and (2) that the $H_{ij}$'s depend on the distance between the two interacting centers both implicitly through $S_{ij}$ and explicitly though $K$. This is the key feature that makes the new version sensitive to bond length variations.

The EH calculations provide as output three energies: (a) the *total energy*, $E_{EH}$, given as a sum of the orbital energies multiplied by the occupation numbers; (b) the *orbital stabilization energy*, $E_{OS}$ where this energy is $E_{EH}$ from which the atomic VOIP of the interacting orbitals are subtracted; (c) the *repulsion energy*, $E_R$. It is usually positive, due to the dominant repulsion between the negatively charged nonbonded atoms.

When tracing the energy variations with the vibrational modes, we use $E_{OS}$ because it reflects the relative energy changes incurred during the geometry conversion relative to the VOIPs.

Three sets of atomic parameters were tested in our calculations (see Appendix).[15-17] The results from these tests are discussed in section 3a.

The approach to constructing the maps by the EH was as follows: A structure with $D_{3h}$ symmetry and fixed axial and equatorial M–L distances is chosen as reference. Then the energy variations with a certain symmetry mode ($\delta S_i$) are traced. The variation is implemented by incrementing the atomic coordinates involved in the mode.

The energy minima, force constants, and vibronic coupling constants were obtained analytically from cubic polynomials fitted to the numerical data (not less than seven points; in most cases over 15 points).

## 3. Results and Discussion

**(a) Choice of Parameters in the Extended Huckel Procedure.** The EH method has a number of limitations (see, e.g. ref 18). A serious limitation is that the EH results depend critically on the choice of parameters and their ability to reflect the variations of the studied properties. To assess the reliability of our EH results several tests were performed.

(i) $E_{SO}$ vs $\delta S_0$ was calculated. $S_0$ is the so-called breathing mode and its variation is defined as

$$\delta S_0 = (1/\sqrt{5})(\delta R_1 + \delta R_2 + \delta R_3 + \delta R_4 + \delta R_5) \quad (4)$$

$\delta R_i$ are the ligand atom displacements. $\delta S_0$ brings about the full dissociation of the ion:

$$[CuCl_5]^{3-} \rightarrow Cu^{2+} + 5Cl^- \quad (5)$$

Three sets of atomic parameters (see Appendix) were tested with respect to eq 5. Set I gave the correct charge separation upon dissociation—$Cu^{2+}$ and $5Cl^-$. Sets II and III gave negative charges on Cu upon $CuCl_5^{3-}$ dissociation, and they were discarded.

In Bresuker et al.'s treatment[12] of $[CuCl_5]^{3-}$ with the standard EH version and set II no such check on the dissociation limit and on the charge separation was made. Judging from our results with the standard EH, the charge distributions produced at large bond distances with this method are not correct.

(ii) The $k$ value in eq 3 may also affect the final results. To assess its impact, $(1 + k)$ was varied from 1.75 to 2.75. From the $E$ vs $\delta S_0$ curves, $R_{min}$ and the force constant $f_0$ were found. $R_{min}$ decreases slightly (2.4–2.3 Å) and the $f_0$ increases more than twice (0.75 → 1.95 mdyn Å$^{-1}$) with increasing $(1 + k)$ without charge iteration. Hence $R_{min}$ is quite insensitive to $(1 + k)$ variations but $f_0$ depends critically on its value. With $k = 2.25$, $R_{min} = 2.41$ Å and $f_0 = 1.09$ mdyn Å$^{-1}$ were obtained. These results compare well with the experimental $R_{min} = 2.3$–$2.4$ Å[2,3] and $f_0 = 0.98$ mdyn Å$^{-1}$ calculated from the 270–280-cm$^{-1}$ band assigned to $\alpha_1'$ vibration.[1]

When charge iteration is included in the procedure, $R_{min}$ rises slighly (less than 0.1 Å) but the $f_0$ drops (0.62 mdyn Å$^{-1}$) because of the reduced atomic charges. Thus charge iteration tends to produce longer bonds and lower force constants. It should be remembered however that the experimental $f_0$ value refers to a *compressed* TBP while $f_0$ calculated from $\delta S_0$ refers to a *regular* TBP.

Standard EH ($H_{ij}$ by eq 1, $K = 2$) with set II produced $R_{min} = 2.70$ Å, and $f_0 = 0.17$ mdyn Å$^{-1}$) which compare unfavorably with the experimental values. This demonstrates in the specific case the inability of the standard EH to produce the energy vs modes maps on which both $R_{min}$ and $f_0$ depend.

To avoid *ad hoc* choices in all calculations $k = 2.25$ and $\Delta = 0.13$ Å$^{-1}$ (default values of the new EH version[15]) were used.

**(b) Preliminary Results from the EH Calculations. Bipyramidal Structure.** The local coordinate axes of the $[CuCl_5]^{3-}$ unit with $D_{3h}$ symmetry are drawn in Figure 2.

The first three highest occupied MOs are[19]

$$e''(xz,yz) < e'(x^2 - y^2,xy) < a_1'(z^2)$$

With nine electrons occupying these orbitals, $^2A_1'$ is the ground state and $^2E'$ and $^2E''$ are the first two excited states, involving

(15) Calzaferri, G.; Forss, L.; Kamber, I. *J. Phys. Chem.* **1989**, *93*, 5366. Calzaferri, G.; Braendle, N. *QCMP* **1993**, 116.
(16) Bakalbassis, E. G.; Mrozinski, J.; Tsipis, C. A. *Inorg. Chem.* **1985**, *24*, 3548.
(17) Hatfield, W. E.; Beddon, H. D.; Horner, S. M. *Inorg. Chem.* **1965**, *4*, 1181.
(18) Murrell, J. N.; Harget, A. J. *Semiempirical Self-consistent-field Molecular-orbital Theory of Molecules*; Wiley-Interscience: New York, 1972.
(19) Rossi, A. R.; Hoffmann, R. *Inorg. Chem.* **1975**, *14*, 365; Allen, G. C.; Hush, N. S. *Inorg. Chem.* **1974**, *6*, 4.

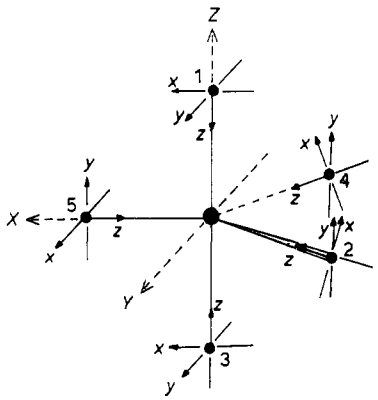

**Figure 2.** Orientation of the local Cartesian coordinates in $ML_5$ with $D_{3h}$ symmetry.

excitations from the filled e′ and e″ MOs to the half-filled $a_1'$ MO, respectively.

For the compressed TBP $[CuCl_5]^{3-}$ unit in the studied compounds the e′ – $a_1'$ separation is about 8000 $cm^{-1}$ and the e″ orbital is lower by about 2000 $cm^{-1}$ than the e′ orbital.[19]

The ground-state electronic configuration for the compressed TBP $[CuCl_5]^{3-}$ with geometry parameters taken from ref 7 is

$$(1a_1)^2(1a_2'')^2(1e')^4(2a_1)^2(3a_1)^2(1e'')^4(4a_1')^2(2e')^4 \times (2a_2'')^2(3e')^4(2e'')^4(a_2')^2(4e')^4(3a_2'')^2(3e'')^4(5e')^4 \times (5a_1')^1(6e')^0(4a_2'')^0(6a_1')^0 \quad (6)$$

The highest occupied MO (HOMO) is $5a_1'$ whose function is

$$\Psi(5a_1') = +0.571(d_{z^2}) + 0.493(p_z^1 + p_z^3) - 0.382(p_z^2 + p_z^4 + p_z^5) \quad (7)$$

in fair agreement with standard EH[12] where the contribution of the $d_{z^2}$ AO to the HOMO was lower by 8%.

It is seen from (7) that the $5a_1'$ MO is bonding to all $Cl^-$ ligands but more strongly to ligands 1,3 (axial) than to ligands 2,4,5 (equatorial). Hence the HOMO reflects the geometry of the compressed TBP used in the calculation. This is a serious test on the EH's sensitivity to the geometric parameters.

**Pyramidal Structure.** The EH calculations with the $C_{2v}$ structure[7] show the expected splitting of the $D_{3h}$ e′ and e″ MOs and the mixing between the new MOs with equal symmetry. The ground state electron configuration for the elongated pyramid is

$$(\text{inner orbitals})^{40}(6b_1)^2(3a_2)^2(b_2)^2(9a_1)^2(10a_1)^1(7b_2)^0 \times (11a_1)^0(7b_1)^0(12a_1)^0 \quad (8)$$

The $5a_1'$ HOMO of the $D_{3h}$ structure in (7) has been transformed into $10a_1$ of the $C_{2v}$ structure. It has acquired five new partners (from the five filled e′ MO) to interact with and one additional partner (unfilled $11a_1$). The $C_{2v}$ HOMO adopts the form

$$\psi(10a_1) = 0.192(d_{x^2-y^2}) + 0.547(d_{z^2}) + 0.488(p_{z^1} + p_{z^3}) - 0.449(p_z^2 + p_z^4) - 0.196(p_z^5) \quad (9)$$

By comparison of (9) with (7) it is seen that the $D_{3h} \rightarrow C_{2v}$ conversion mixes the Cu $d_{x^2-y^2}$ orbital to the new HOMO. In it Cu $d_{x^2-y^2}$ is antibonding with respect to ligand 5 and bonding with respect to ligand 2 and 4 (see Figure 3). The axial bonds are unaffected by the conversion—the coefficients of Cu $d_{z^2}$ and $p_z^1$, $p_z^3$ in the old and new HOMOs are practically the same—a feature that is inherent in the real geometries used in the calculations.

Having obtained definite proof that the MOs reflect the input geometries, the energy changes will be traced now (see Table 1).

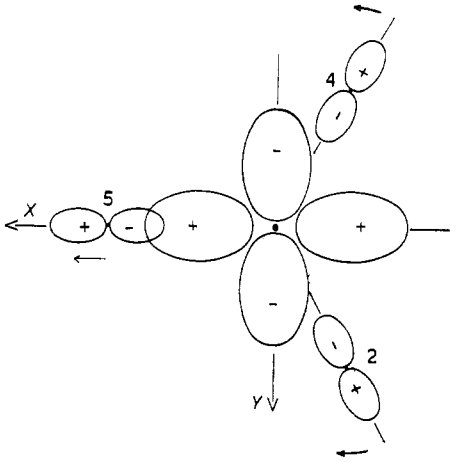

**Figure 3.** Illustration of how the increased contribution of the Cu $d_{x^2-y^2}$ AO (0% in $D_{3h}$ and 4% in $C_{2v}$) to the HOMO affects the distortion in the equatorial plane. Atoms 2 and 4 move away from each other and open the $Cl^2CuCl^4$ angle, and their p AOs increase bonding overlap with the Cu $d_{x^2-y^2}$ AO. In this way the $CuCl^2$ and $CuCl^4$ bonds may become shorter.

**Table 1.** Energy Data (in eV) for the Two $CuCl_5^{3-}$ Units with Real Geometries

| | compressed TBP | elongated pyramid | difference EP – CTBP |
|---|---|---|---|
| sum of orbital energy | –930.4139 | –931.3141 | –0.9002 |
| orbital stabilization | –47.9573 | –48.0646 | –0.1073 |
| repulsion energy | 0.4464 | +0.4564 | +0.0100 |
| repulsion + stabilization | –47.5109 | –47.6082 | –0.0973 |
| $q_{Cu}$ | 0.209 | 0.221 | –0.012 |
| $q_{Cl}^{1,3}$ | –0.569 | –0.569 | 0.000 |
| $q_{Cl}^{2,4}$ | –0.691 | –0.610 | 0.081 |
| $q_{Cl}^{5}$ | –0.691 | –0.863 | –0.172 |
| LUMO | 0.3593 | –2.3978 | –2.7571 |
| HOMO | –11.7274 | –11.6450 | 0.0824 |

Energy differences of ±0.01 eV are believed to be significant. From this table it is seen that *in terms of the EH method* the $C_{2v}$ pyramid is the lower energy structure; its energy is by 0.9 eV lower than that of the $D_{3h}$ compressed TBP. The values in this table reveal the origin of the energy gain: (i) orbital stabilization is responsible for only 12% of the energy drop; (ii) the increase in repulsion energy for $D_{3h} \rightarrow C_{2v}$ is a very minor factor, opposing the conversion; (iii) the largest factor is the *orbital interaction* leading to stronger bonds for the lower symmetry structure. This is typically a PJTC manifestation as discussed in detail by Polinger et al.[12]

This problem is pursued further to elucidate the origin of the orbital energy depression upon distorting the TBP structure. As noted the $D_{3h}$ $5a_1'$ HOMO is transformed into the $C_{2v}$ $10a_1$ HOMO. In doing so it is *raised* by about 0.08 eV and becomes slightly more *antibonding* than the $D_{3h}$ HOMO (see eqs 7 and 9). Figure 3 shows how the admixing of Cu $d_{x^2-y^2}$ increases the antibonding nature of the new HOMO. The EH matrix in $C_{2v}$ reveals that the largest mixing of the transformed HOMO is with the $a_1$ component of the $D_{3h}$ 2e′-bonding MO ($5a_1'$–2e′ energy separation is 4.01 eV); 2e′ has the highest percentage of Cu $d_{x^2-y^2}$ (50%). Conversely, the highest occupied 5e′ is split by 0.2 eV upon the TBP distortion; its $a_1$ component has a much lower percentage of Cu $d_{x^2-y^2}$.

**(c) Symmetry Treatment of the Pseudo-Jahn–Teller Problem.** The molecular frames and the numbering of the atoms in the $[CuCl_5]^{3-}$ unit were given in Figure 1. The symmetry modes $S_i$ of $ML_5$ with $D_{3h}$ and $C_{2v}$ symmetry in terms of internal coordinates, obtained by projection operators, are listed in Tables 2 and 3. Figure 4 depicts their shapes. They coincide with those reported elsewhere[20,21] for $D_{3h}$ but differ from the ill-defined polar

**Table 2.** Symmetry Coordinates of $ML_5$ with $D_{3h}$ Symmetry in Terms of Internal Coordinates $(2\alpha_1' + 2\alpha_2'' + 3\epsilon' + \epsilon'')^a$

| | IR | symmetry mode | displaced point group symmetry |
|---|---|---|---|
| $S_1$ | $\alpha_1'$ | $2^{-1/2}(R_1 + R_3)$ | $D_{3h}$ |
| $S_2$ | $\alpha_1'$ | $3^{-1/2}(R_2 + R_4 + R_5)$ | $D_{3h}$ |
| $S_3$ | $\alpha_2''$ | $2^{-1/2}(R_1 - R_3)$ | $C_{3v}$ |
| $S_4$ | $\alpha_2''$ | $6^{-1/2}(\alpha_{12} + \alpha_{14} + \alpha_{15} - \alpha_{34} - \alpha_{23} - \alpha_{35})R$ | $C_{3v}$ |
| $S_5$ | $\epsilon'_a$ | $6^{-1/2}(2R_5 - R_4 - R_2)$ | $C_{2v}$* |
| $S_6$ | | $2^{-1/2}(R_4 - R_2)$ | $C_5$ |
| $S_7$ | $\epsilon'_b$ | $6^{-1/2}(2\alpha_{24} - \alpha_{25} - \alpha_{45})R$ | $C_{2v}$* |
| $S_8$ | | $2^{-1/2}(\alpha_{25} - \alpha_{45})R$ | $C_s$ |
| $S_9$ | $\epsilon'_c$ | $12^{-1/2}(2\alpha_{15} - \alpha_{14} - \alpha_{12} + 2\alpha_{35} - \alpha_{34} - \alpha_{23})R$ | $C_{2v}$* |
| $S_{10}$ | | $^1/_2(\alpha_{14} - \alpha_{12} + \alpha_{34} - \alpha_{23})R$ | $C_s$ |
| $S_{11}$ | $\epsilon''$ | $12^{-1/2}(2\alpha_{15} - \alpha_{14} - \alpha_{12} - 2\alpha_{35} + \alpha_{34} + \alpha_{32})R$ | $C_s$ |
| $S_{12}$ | | $^1/_2(\alpha_{14} - \alpha_{12} - \alpha_{34} + \alpha_{32})R$ | $C_1$ |

[a] The $\epsilon'$ modes marked by "*" are used in the calculations.

**Table 3.** Symmetry Coordinates of $ML_5$ with $C_{2v}$ Symmetry in Terms of Internal Coordinates $(5\alpha_1 + \alpha_2 + 3\beta_1 + 3\beta_2)$

| | IR | symmetry mode | displaced point group symmetry[a] |
|---|---|---|---|
| $S_1$ | $\alpha_1$ | $R_5$ | $C_{2v}$ |
| $S_2$ | $\alpha_1$ | $2^{-1/2}(R_1 + R_3)$ | $C_{2v}$ |
| $S_3$ | $\alpha_1$ | $2^{-1/2}(R_2 + R_4)$ | $C_{2v}$ ($\epsilon_a'$)* |
| $S_4$ | $\alpha_1$ | $2^{-1/2}(\alpha_{15} + \alpha_{35})R$ | $C_{2v}$ ($\epsilon_b'$)* |
| $S_5$ | $\alpha_1$ | $2^{-1/2}(\alpha_{25} + \alpha_{45})R$ | $C_{2v}$ ($\epsilon_c'$)* |
| $S_6$ | $\alpha_2$ | $^1/_2(\alpha_{12} - \alpha_{14} - \alpha_{23} + \alpha_{34})R$ | $C_1$ ($\epsilon''$) |
| $S_7$ | $\beta_1$ | $2^{-1/2}(R_1 - R_3)$ | $C_1$ |
| $S_8$ | $\beta_1$ | $2^{-1/2}(\alpha_{15} - \alpha_{35})R$ | $C_s$ |
| $S_9$ | $\beta_1$ | $^1/_2(\alpha_{12} + \alpha_{14} - \alpha_{23} - \alpha_{34})R$ | $C_s$ ($\epsilon''$) |
| $S_{10}$ | $\beta_2$ | $2^{-1/2}(R_2 - R_4)$ | $C_s$ ($\epsilon_a'$) |
| $S_{11}$ | $\beta_2$ | $2^{-1/2}(\alpha_{25} - \alpha_{45})R$ | $C_s$ ($\epsilon_c'$) |
| $S_{12}$ | $\beta_2$ | $^1/_2(\alpha_{12} - \alpha_{14} + \alpha_{23} - \alpha_{34})R$ | $C_s$ ($\epsilon_b'$) |

[a] In parentheses the corresponding $D_{3h}$ modes.

coordinates reported in ref 11. The correct polar coordinate for the equatorial displacements are given in ref 22.

For a $d^9$ ion located in a ligand field with $D_{3h}$ symmetry the PJTC problem is $^2A_1' \otimes \epsilon' \otimes {}^2E$. Hence the three $\epsilon'$ modes may be PJTC active. Tables 2 and 3 list in the last column the displaced point group symmetry. Figure 5 gives the symmetry descent[9] (subduction) from $D_{3h}$ and the fate of the degenerate modes, $\epsilon'$ and $\epsilon''$ in the lower symmetry groups.

By definition the epikernel[23] is the subduced group where *one* of the degenerate mode components is transformed into a totally symmetric mode, *i.e.* stereochemically inactive. Stationary points correspond to epikernels only.[23]

As seen from Tables 2 and 3 and Figure 5 the only epikernel starting with reference symmetry $D_{3h}$ is $C_{2v}$. The $C_{4v}$ symmetry should be excluded as a stationary point. The correlation between $D_{3h}$ and $C_{2v}$ that can help to understand the changes in symmetry of the modes (Figure 5) is given in Table 4. A detailed and lucid discussion of the idealized five-coordinate conformations can be found in ref 21.

Several important results follow right from the start by inspecting Tables 2 and 3 and Figures 4 and 5.

(i) The three $\epsilon'$-modes of $ML_5$ with $D_{3h}$ symmetry lower the symmetry of $ML_5$ to $C_{2v}$ ($S_5$, $S_7$, $S_9$) and $C_s$ ($S_6$, $S_8$, $S_{10}$). Since

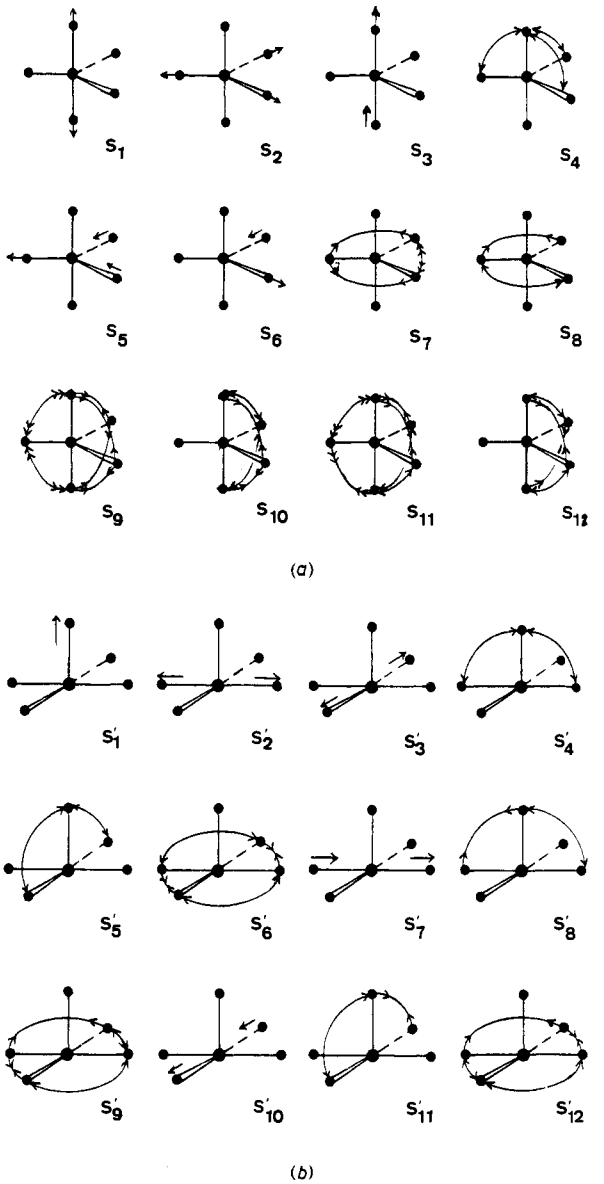


**Figure 4.** Symmetry coordinates: (a) in $D_{3h}$; (b) in $C_{2v}$ (see Tables 2 and 3). The double-headed arrows represent a double displacement as compared with that denoted by single-headed arrows.

$C_{2v}$ is epikernel and $C_s$ is not, the $C_{2v}$-producing component of the $\epsilon'$ mode should be the only mode component to be considered in the geometry transformation.

The linear vibronic coupling element is (in $D_{3h}$ notations)

$$\sum\sum\left\langle \Psi(^2A_1')\left|\frac{\partial V}{\partial S_{\epsilon'}}\right|\Psi(^2E')\right\rangle \qquad (10)$$

where the sums are taken over the components of the $^2E'$ states and the components of the $\epsilon'$ modes.

Taking into account Table 4 the sum can be written in $C_{2v}$ as

$$\left\langle \Psi(^2A_1)\left|\frac{\partial V}{\partial S_{\alpha_1}}\right|\Psi(^2A_1)\right\rangle + \left\langle \Psi(^2A_1)\left|\frac{\partial V}{\partial S_{\beta_2}}\right|\Psi(^2A_1)\right\rangle + \left\langle \Psi(^2A_1)\left|\frac{\partial V}{\partial S_{\alpha_1}}\right|\Psi(^2B_2)\right\rangle + \left\langle \Psi(^2A_1)\left|\frac{\partial V}{\partial S_{\beta_2}}\right|\Psi(^2B_2)\right\rangle \qquad (11)$$

Only the first term is nonvanishing by symmetry, proving the claim that only the $C_{2v}$-producing components of $S_{\epsilon'}$ ($S_{\alpha_1}$ in $C_{2v}$) should be considered in the vibronic coupling calculations.

(20) Bartell, L. S.; Plato, V. *J. Am. Chem. Soc.* **1973**, *95*, 3097.
(21) Auf-der-Heyde, T. P. E.; Burgi, H.-B. *Inorg. Chem.* **1989**, *28*, 3960, 3970, 3982.
(22) Ceulemans, A. In *Vibronic Processes in Inorganic Chemistry*; Flint, C. D., Ed.; Kluwer Acad. Publ.: Dordrecht, The Netherlands 1989; p 221.
(23) Ceulemans, A.; Vanquickenborne, L. *Struct. Bonding* **1989**, *71*, 126. Ceulemans, A.; Beyens, D.; Vanquickenborne, L. *J. Am. Chem. Soc.* **1984**, *106*, 5824. See also: Liehr, A. D. *J. Phys. Chem.* **1963**, *67*, 389.

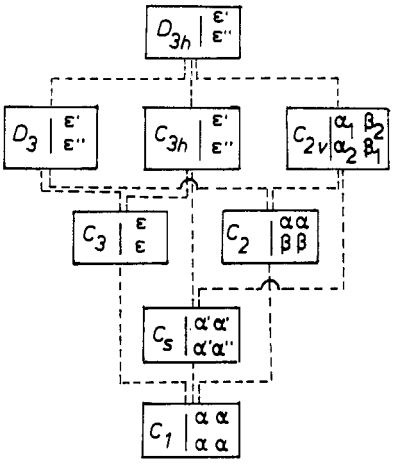


**Figure 5.** Symmetry descent of TBP ($D_{3h}$) and the transformation of the $\epsilon'$ and $\epsilon''$ symmetry modes (Greek letters). The epikernel of a given mode is the symmetry group for which *one* mode component transforms as the totally symmetric $\alpha_1$, $\alpha$, or $\alpha'$ mode.

(ii) The PJTC in $D_{3h}$ symmetry can be formulated in terms of the interacting orbitals[10] as follows: $a_1' \otimes 3\epsilon' \otimes e'$, where $a_1'$ and $e'$ are the interacting orbitals and $\epsilon'$ are the PJTC active vibrations. The full $D_{3h}$ orbital interaction matrix involves *all* $a_1'$ and $e'$ MOs. The full $C_{2v}$ matrix sorts out *all* the $a_1$ components. In view of the symmetry arguments discussed above, the PJTC interaction matrix may be further factored out with respect to the vibrational modes by taking into account only the $C_{2v}$ components of the $\epsilon'$ modes.

Using the $C_{2v}$ components of the $\epsilon'$ modes, the PJTC problem $a_1' \otimes 3\epsilon' \otimes e'$ is reduced from 6-dimensional to 3-dimensional one with respect to the symmetry modes involved.

(iii) It follows from point ii that the difference between the Berry twist mechanism (Berry pseudorotation)[24] and the full PJTC consists in which $\epsilon'$ modes are used: In the Berry mechanism only the bending modes ($S_7$ and $S_9$ in our case) are active; in this manner axial and equatorial positions become equivalent. The full PJTC is more general and may involve *all three* $\epsilon'$ modes in *any* combination.

(iv) The genuine JTC in the excited state $^2E'$ is $e' \otimes 3\epsilon'$, where $e'$ represents one hole in the lower lying $e'$ MOs. The new $^2A_1$ states produced in this way from $e' \rightarrow a_1'$ excitations can mix with the ground-state $^2A_1$ term in $C_{2v}$ through a JT (vibronically) induced *configuration interaction mechanism.*

Since $\epsilon'$ are the active mode in both PJTC and genuine JTC cases the real case should be a mixed (PJTC ⊕ JTC) one. In the present work the genuine JTC is ignored.

The excited states $^2E''$ give rise to the genuine JTC problem $e'' \otimes 3\epsilon'$ leading to $^2A_1''$, $^2A_2''$, $^2E''$ vibronic states, none of which can be transformed into $^2A_1$ in the epikernel $C_{2v}$; hence, the $^2E''$ states cannot participate in the JTC.

**(d) The TBP Ground State $^2A_1'$ Term in the Subspace of the Two Totally Symmetric Modes.** The two $\alpha_1'$ modes ($S_1$ and $S_2$, see Table 2) retain the TBP symmetry $D_{3h}$ if these modes perform either separately or in any combination. Two dissociation paths however can be discerned

$$[CuCl_5]^{3-} \rightarrow [CuCl_3]^- + 2Cl^- \qquad (12)$$

when the axial bonds are ruptured by $\delta S_1$ and a planar 3-coordinate ion $[CuCl_3]^-$ is obtained and

$$[CuCl_5]^{3-} \rightarrow CuCl_2 + 3Cl^- \qquad (13)$$

when the equatorial bonds are ruptured by $\delta S_2$ and a linear molecule $CuCl_2$ is formed.

(24) Berry, R. S. *J. Chem. Phys.* **1960**, *32*, 933. *Rev. Mod. Phys.* **1960**, *32*, 447. Zwanziger, J. W.; Koenig, M.; Pines, A. *Annu. Rev. Phys. Chem.* **1990**, *41*, 691.

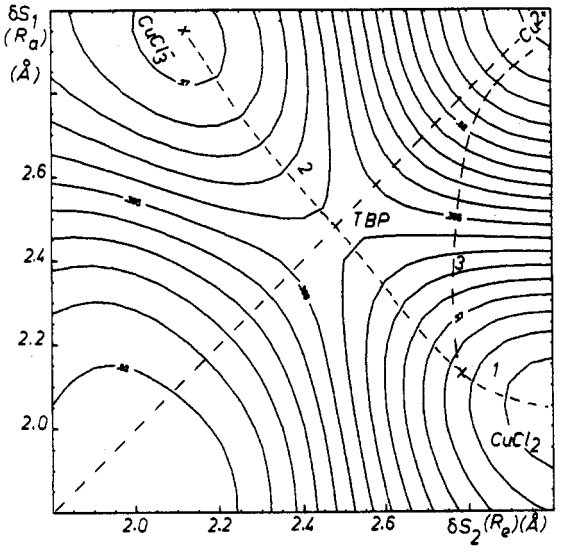


**Figure 6.** Map of the ground-state orbital stabilization energy vs. $\delta S_1$ and $\delta S_2$ ($\alpha_1'$ modes). The regular TBP is a saddle point with $R_{ax} = R_{eq}$ = 2.52 Å and −930.76-eV energy taken as reference zero. There are three dissociative pathways: (1) to $CuCl_2 + 3Cl^-$, (2) to $CuCl_3^- + 2Cl^-$, and (3) to $Cu^{2+} + 5Cl^-$. $R_a$ ($R_1$,$R_3$) and $R_e$ ($R_2$,$R_4$,$R_5$) denote the incremented value in the two $\alpha_1'$ modes. Note the location of the compressed TBP point.

**Table 4.** Correlation between $D_{3h}$ and $C_{2v}$

| $D_{3h}$ | $\alpha_1'$ | $\alpha_2'$ | $\epsilon'$ | $\alpha_1''$ | $\alpha_2''$ | $\epsilon''$ |
|---|---|---|---|---|---|---|
| $C_{2v}(\sigma_h \rightarrow \sigma_{zy})$ | $\alpha_1$ | $\beta_2$ | $\alpha_1 + \beta_2$ | $\alpha_2$ | $\beta_1$ | $\alpha_2 + \beta_1$ |

If $CuCl_2$ and $[CuCl_3]^-$ were stable species in the $CuCl_5$ conformational space they should appear as separate minima on the $\alpha_1'$ map.

Two combinations of $S_1$ and $S_2$ are possible.

(i) The in-phase combination $c_1\delta S_1 + c_2\delta S_2$, where $c_i$ are the mixing coefficients taken to be positive, produces full dissociation of the $[CuCl_5]^{3-}$ species (eq 5).

(ii) The out-of-phase combination $c_1\delta S_1 - c_2\delta S_2$, where $c_i$ are also positive but differ in general from those in the in-phase combination. It is exactly this case which, depending on the absolute values of $c_i$ *and* the sign of the resulting gradient, can distort the regular TBP to a *compressed* or *elongated* TBP.

The role of the two $\alpha_1'$ modes will be further enlarged in conjunction with the PJTC modes, but the $\alpha_1'$ modes are first treated separately; *i.e.*, the $D_{3h}$ symmetry is a valid constraint.

The $E$ vs $\delta S_1$, $\delta S_2$ map is shown in Figure 6. The dashed line represents the special case $\delta S_1 = \delta S_2$, *i.e.* a *regular* TBP. In this case the energy minimum occurs at $R_{eq} = R_{ax} = 2.52$ Å.

Relaxing the constraing $\delta S_1 = \delta S_2$ and considering the general case where $\delta S_1 \neq \delta S_2$, this point is no longer a minimum: the regular TBP can distorts with no energy barrier to a *compressed* TBP (see Figure 6) with $R_{ax}$ = 2.15 Å and $R_{eq}$ = 2.75 Å, compression ratio 0.78 (compare with the experimental $R_{ax}$ = 2.300 and $R_{eq}$ = 2.394 Å,[7] compression ratio 0.96). The energy gain accompanying the compression is 1.7 eV, and the driving force at the regular TBP's energy minimum point along this path is −6.0 eV Å$^{-1}$. Figure 7 shows part of the map illustrating the position of the compressed TBP. The shallow minimum appears on the descending slope of along the $CuCl_2 + 3Cl^-$ dissociation path.

Renouncing the charge iteration procedure improves the calculated bond distances (2.25 and 2.55 Å, equatorial and axial bonds, respectively, compression ratio 0.88), but the energy gain is reduced by 1 eV.

There is no minimum on the entire $\alpha_1'$ map corresponding to an elongated TBP. Hence the compressed TBP is the only species that may exist in the absence of PJTC. This result contradicts

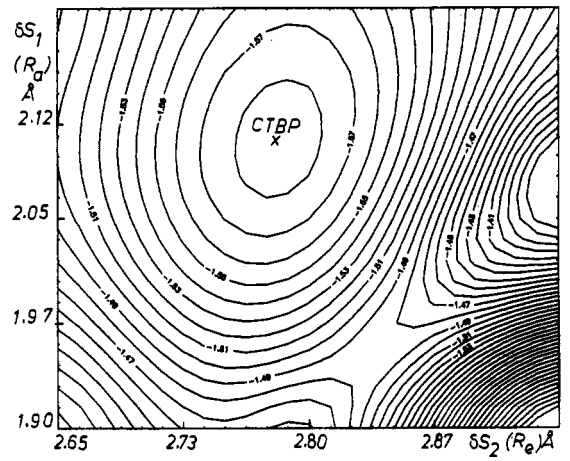


**Figure 7.** Excerpt of Figure 6 showing the location of the compressed TBP point and the surrounding rim.

the interligand repulsion[25] and molecular mechanics[26] calculations which in the absence of electronic effects predict the elongated TBP to be more stable than the compressed. It is particularly important to note that the compression of $[CuCl_5]^{3-}$ follows from the $D_{3h}$ ground state electronic configuration (one hole in $a_1'$ where $d_{z^2}$ is dominant); i.e., it is an electronic effect.

The compressed TBP $[CuCl_5]^{3-}$ ion can take three pathways to partial or complete dissociation.

**Path 1—Equatorial Expansion with Slight Axial Compression To Form the Linear $CuCl_2$ and 3 $Cl^-$.** To get along this pathway an energy barrier of 0.11 eV (about 900 $cm^{-1}$) must be surmounted. The gain in orbital energy produced by dissociating the compressed TBP to $CuCl_2$ and three $Cl^-$ is 7.1 eV.

**Path 2—Axial Elongation with Subsequent and Parallel Equatorial Compression To Form a Triangular $[CuCl_3]^-$ ($R$ = 2.15 Å) with 2 $Cl^-$.** To reach this point the compressed TBP $[CuCl_5]^{3-}$ unit must pass over the barrier of the regular TBP (8.8 eV loss). Hence this path is energetically unfavorable.

**Path 3—Total Dissociation.** It takes $[CuCl_5]^{3-}$ over a path with $R_e$ = 2.8 Å constant until $R_a$ = 2.6 Å is reached and then joins the path along the breathing mode. This path has an energy barrier of about 2.7 eV. The net orbital energy gain is about 16 eV. This is the energy of formation for the $[CuCl_5]^{3-}$ ion.

The locations of the minima in Figures 6 and 7 were not altered much when using slightly different atomic parameters. Renouncing the explicit distance dependence of $H_{ij}$ (eq 2) and resorting to the standard EH, however, gave a global orbital energy minimum for a *regular* TBP with $R$ = 2.7 Å at a much higher energy (by 70 eV). The dissociation limit is reached for $Cu^{3-}$ and neutral chlorine atoms.

It may be thus concluded that the compressed TBP is an intrinsic feature of the $[CuCl_5]^{3-}$ ion. It results from the action of the two $\alpha_1'$ modes in the absence of PJTC and is most likely due to the asymmetry in the filled Cu d AOs.[12]

**(e) The Multimode Pseudo-Jahn–Teller Couplings $A_1' \otimes (2\alpha_1' \oplus 2\epsilon') \otimes E'$ and $A_1' \oplus (2\alpha_1' \oplus 3\epsilon') \otimes E''$.** The impact of the $C_{2v}$-components of the three $\epsilon'$-modes ($S_5, S_7, S_9$) on the geometries of the $[CuCl_5]^{3-}$ unit will be traced. To avoid introducing severe restrictions that may affect the final results the following procedure is adopted: the $E_{OS}$ energy maps vs $\delta S_7$, $\delta S_9$ (bending modes) are mapped by treating $S_5$ (stretching mode) as a parameter. The two $\alpha'$ modes are included as a series of instant snapshots: compressed TBP, regular TBP, and elongated TBP are treated as reference structures.

**4. Problems. (I) The Problem $A_1' \otimes (2\alpha_1' \oplus 2\epsilon') \otimes E'$.**

It includes the two bending $\epsilon'$ – modes with the restriction $\delta S_5 = 0$ (no bond stretching). This is in fact the genuine Berry twist which involves only bending modes.[24]

Figure 8 shows the E vs. $\delta S_7$, $\delta S_9$ maps for compressed (a), regular (b) and elongated (c) TBP.

**In-phase $\alpha_1'$ Combination. $\delta S_5 = 0$ (Berry Pseudorotation). Regular TBP (Figure 8b).** Two isoenergetic TBP global minima and a SP ($C_{4v}$) saddle point with Cl(apical)CuCl(basal) = 102° are present; in fact $C_{4v}$ constitutes the energy barrier along the two TBP interconversion paths. Figure 8b reproduces almost exactly the ILR energy vs the $\delta S_7$, $\delta S_9$ map (see ref 25, Figures 4.2a and 4.2b). The energy barrier ($C_{4v}$ point) is about 0.06 eV (480 $cm^{-1}$) for $R$(Cu–Cl) = 2.4 Å, and it increases with decreasing Cu–Cl bond length. It should be emphasized that the square pyramid is not a minimum on this map. It can be formed as a thermal average from the two *regular* differently oriented TBPs under the combined action of the two $C_{2v}$-producing $\epsilon'$ modes. This is exactly the opposite of what was supposed from AOM results,[1,8] and it points to a sign error (choice of phases) in these AOM calculations.

**Out-of-Phase $\alpha_1$ Combination. $\delta S_5 = 0$ (Berry Pseudorotation). (a) Compressed TBP.** Figure 8a illustrates the $E$ vs $\delta S_7$, $\delta S_9$ map for a TBP compressed in advance. This figure shows a remarkable result: the compressed TBP is no longer the global minimum as was the case with the regular TBP; it is a high-energy local minimum. When subjected to the combined effect of the two $\epsilon'$ bending modes ($\delta S_7$, $\delta S_9$) the compressed TBP slides toward a distorted SP structure with $C_{2v}$ symmetry. In fact it is the pyramidal ($C_{2v}$) structure that is the global minimum in the studied case.

To get along the $C_{2v}$ path, the initially *compressed* TBP structure has to overcome the rim of the local $D_{3h}$ minimum which amounts to a low-energy barrier of about 0.015–0.020 eV (120–150 $cm^{-1}$, thermally accessible). After getting over the energy barrier, the driving force for the compressed TBP to distort further to the $C_{2v}$ structure is high—about –4.3 eV $Å^{-1}$.

The resulting $C_{2v}$ structure occurs at $\delta\theta$ = 22° ($Cl^1CuCl^3$ = 136°) and $\delta\phi$ = –30° ($Cl^2CuCl^4$ = 180°). This is structure **2**—ligands 2,4 are axial, and ligands 1,3,5 are equatorial. It is a TBP structure with three longer bonds ($CuCl^2$ and $CuCl^4$ axial; $CuCl^5$ equatorial) and two shorter bonds ($CuCl^1$ and $CuCl^3$ now equatorial, being axial prior to the $D_{3h} \rightarrow C_{2v}$ distortion).

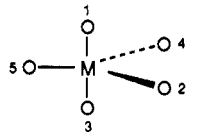


compressed TBP ($D_{3h}$)

**1**

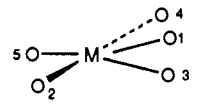


elongated pyramid ($C_{2v}$)

**2**

The $C_{2v}$ structure can also be termed as elongated pyramidal with one long bond ($CuCl^5$) at the apex and the two unequal trans basal angles $Cl^2CuCl^4$ = 180° and $Cl^1CuCl^3$ = 136°; these value are very nearly (179 and 146°) the experimental angles observed in the low-temperature phase of $[Co(NH_3)_6][CuCl_5]$ where $[CuCl_5]^{-3}$ has $C_{2v}$ symmetry.[7] Structure **2**, while reproducing satisfactorily the angular features of the real $C_{2v}$ structure, is still lacking with respect to the real bond lengths: to obtain the real structure, **2** has to be compressed along the $CuCl^2$ and $CuCl^4$ bonds.

Starting with a *compressed* TBP, a structure with $C_{4v}$ symmetry is not possible at all if only bending motion is involved: $\delta S_7$ and $\delta S_9$ make the TBP's shorter axial bonds become trans basal and they would differ in length from the other trans basal bonds formed from the former TBP's longer equatorial bonds.

(25) Kepert, D. L. *Inorganic Stereochemistry*; Springer Verlag: Berlin, 1982. Favas, M. C.; Kepert, D. L. *Prog. Inorg. Chem.* **1980**, *27*, 325. McDowell, H. K.; Chiu, H.-L.; Geldard, J. F. *Inorg. Chem.* **1988**, *27*, 1674.
(26) Rodger, A.; Schipper, P. E. *Inorg. Chem.* **1988**, *27*, 458.

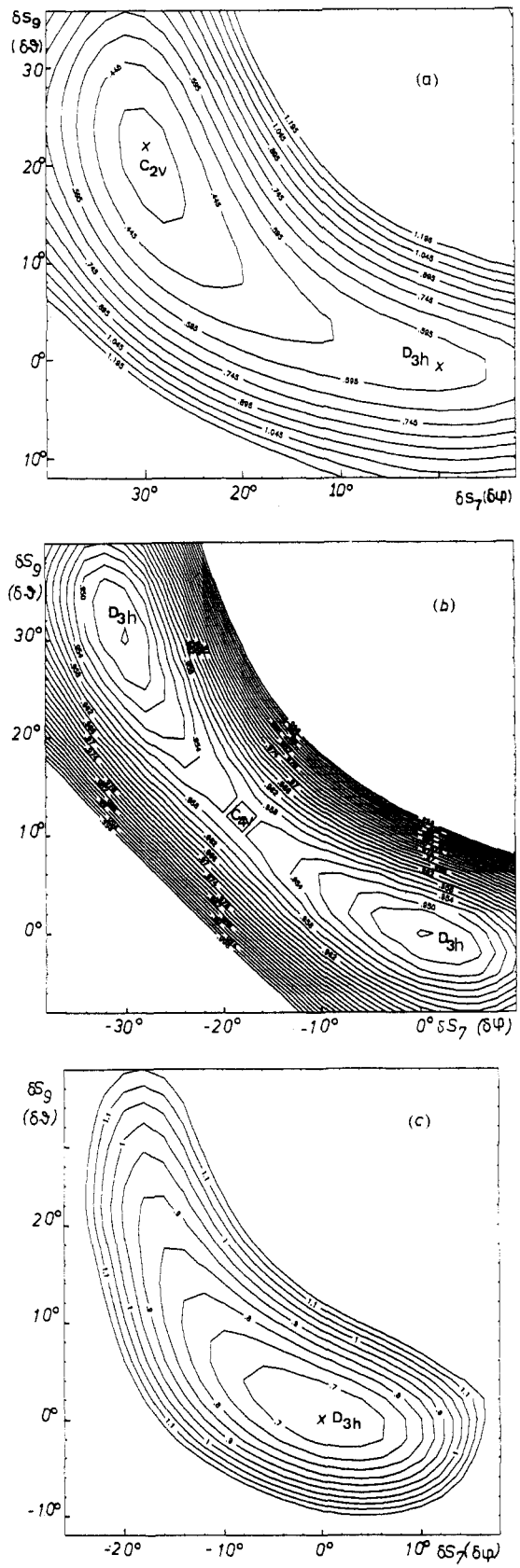


**Figure 8.** Map of the ground-state orbital stabilization energy vs $\delta S_7$ and $\delta S_9$ (the two bending $C_{2v}$-producing $\epsilon'$ modes): (a) compressed TBP with $R_{ax}$ = 2.3 Å and $R_{eq}$ = 2.4 Å; (b) regular TBP with $R_{ax} = R_{eq}$ = 2.4 Å; (c) elongated TBP with $R_{ax}$ = 2.4 Å and $R_{eq}$ = 2.3 Å. $\delta\phi$ and $\delta\theta$ denote the incremented values in $\delta S_7$ and $\delta S_9$, respectively.

The net energy gain on $D_{3h}$ (compressed TBP) → $C_{2v}$ conversion is 0.24 eV (about 2000 cm$^{-1}$). This is the PJTC stabilization energy produced by the bending $\epsilon'$ modes, operating in conjunction with the out-of-phase combination of the $\alpha_1'$ modes. The same value was obtained by the AOM[10,11] within a quite different approach, using different sets of symmetry coordinates and force constants and neglecting the totally symmetric modes. For this reason and because of the AOM's inability to treat PJTC problems,[12] the coincidence may be fortuitous.

The exact location of the new global $C_{2v}$ minimum depends on the TBP compression ratio. For compression ratios ranging from 0.8 to 0.95, the new $C_{2v}$ structure always occurs with $\delta\phi \sim -30°$ but variable $\delta\theta \sim$ 20–30°, *i.e.* values close to the experimental ones.[7]

**(b) Elongated TBP.** There is no minimum on the $\alpha_1'$ sheet for the elongated TBP (see Figure 6). Figure 8c shows that there is also no energy gain when subjecting an elongated TBP to the action of the bending $\epsilon'$ modes $\delta S_7$, $\delta S_9$.

This difference in the behavior of the compressed and elongated TBP's demonstrates the very important promotive role of the totally symmetric modes in an out-of-phase combination in shaping the $[CuCl_5]^{3-}$ geometry.

**(c) Comparison of the Compressed, Regular, and Elongated TBPs.** By comparing Figure 8a (compressed TBP) with Figure 8b (regular TBP) and Figure 8c (elongated TBP) one can see the three-stage action of the $\alpha_1'$ out-of-phase combination in conjunction with the $\epsilon'$ bending modes when the stretching $\epsilon'$ mode is inoperative ($\delta S_5 = 0$): compression pushes the TBP to convert to an elongated pyramid ($C_{2v}$); the regular TBP produces two regular TBP global minima and one SP ($C_{4v}$) saddle point; elongation stabilizes the TBP as such but at energies higher than those for the elongated pyramidal ($C_{2v}$) and compressed TBP ($D_{3h}$) structures. Hence the $\alpha_1'$ out-of-phase combination in conjunction of the $\epsilon'$ bending mode should stabilize the $[CuCl_5]^{3-}$ unit in the elongated pyramidal form ($C_{2v}$).

**(II) The Multimode Problem $A_1' \otimes (2\alpha_1' \oplus 3e') \otimes E'$. Effect of the Stretching $\epsilon'$-Mode ($S_5$).** The $\delta S_5$ mode yields $C_{2v}$ as displaced symmetry.

To obtain the real $C_{2v}$ structure from an initially compressed TBP with $R_{eq}$ = 2.43 Å, $\delta S_5$ should act with $\delta R$ = 0.083 Å. It remains to be seen whether a minimum appears in the $\delta S_5$, $\delta S_7$ or $\delta S_5$, $\delta S_9$ maps.

Three different reaction routes are depicted in Figure 9. A regular TBP with $R_{ax} = R_{eq}$ = 2.43 Å is chosen as the parent structure in order to reproduce the final $C_{2v}$ structure with $\delta S_5$ ($\delta R$ = 0.83 Å) in paths B and C, but any other parent TBP may be used in route C with different increments.

**Route A.** The first step, $\delta S_1$ and $\delta S_2$, is axial compression and equatorial expansion effected by the $\alpha_1$ modes. It is accompanied by a 0.934-eV energy gain. The next step is the Berry twist—$\delta S_7$ and $\delta S_9$ exchange axial with equatorial ligands. It occurs with a 0.009-eV energy loss. New axial compression ($\delta S_1$) ultimately yields the experimental $C_{2v}$ structure with a 0.174-eV energy loss. The overall energy gain on going from the *regular* TBP to the experimental $C_{2v}$ structure is 0.751 eV. Note that for the conversion of an already compressed TBP to the $C_{2v}$ structure the energy gain is 0.90 eV (Table 1). The incremental values in the symmetry mode variations are large.

**Route B.** Berry pseudorotation ($\delta S_7$, $\delta S_9$) is the first step with a 0.297-eV energy gain. In the next step the new axial bonds are compressed ($\delta S_1$) with a 0.042-eV energy loss; finally there is equatorial stretching ($\delta S_5$) which makes the new equatorial bonds inequivalent with a 0.497-eV energy gain. The order of the last two stages may be reverse.

**Route C.** It involves axial compression ($\delta S_1$) with almost no energy change (0.01-eV gain), stretching in the equatorial plane ($\delta S_5$) with a 0.167-eV energy gain and finally bending in the same plane ($\delta S_7$) with a 0.573-eV energy gain.

Routes A and B are less probable than route C. This claim is based on the following arguments.

(i) Route A involves axial compression, which is energetically favorable (Figure 6). However, the next two steps produce higher

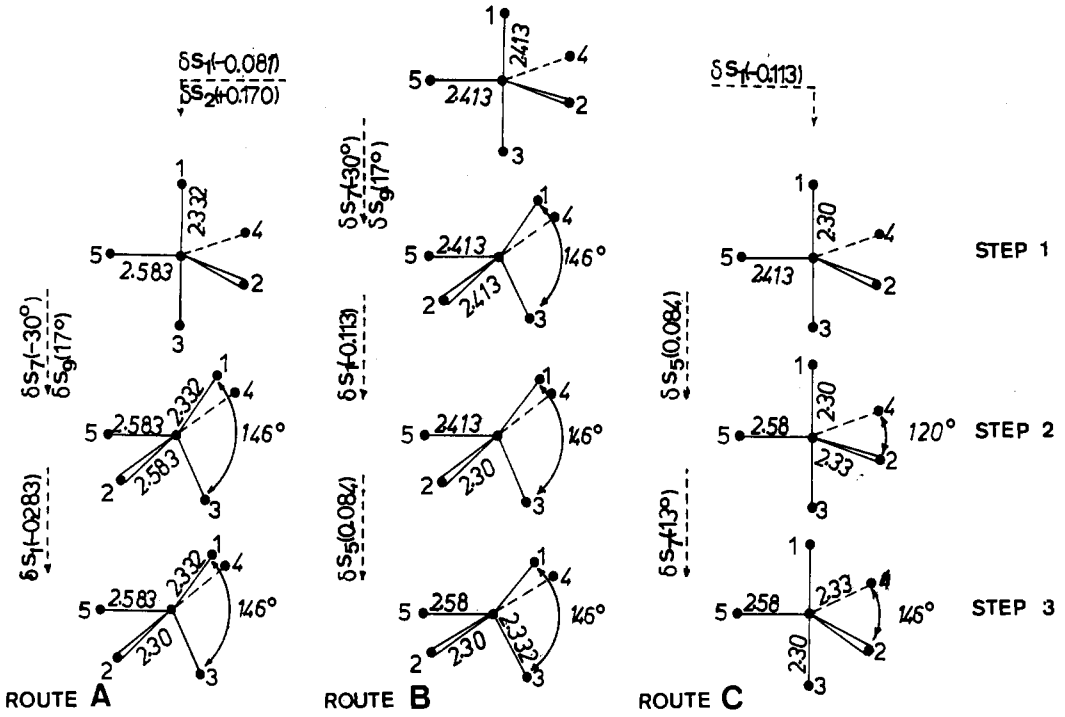


**Figure 9.** The three routes of shaping the compressed TBP ($D_{3h}$) and the elongated pyramid ($C_{2v}$) structures from a parent regular TBP. $\delta S_i$ denote the symmetry modes; $\delta R$, $\delta\phi$, and $\delta\theta$ stand for the increments in the symmetry modes. Route A, ($\delta S_1$, $\delta S_2$) → ($\delta S_7$, $\delta S_9$) → $\delta S_1$; Route B, ($\delta S_7$,$\delta S_9$) → $\delta S_1$ → $\delta S_5$; Route C, $\delta S_1$ → $\delta S_5$ → $\delta S_7$. Note that routes A and B involve Berry twist ($\delta S_7$, $\delta S_9$) that exchanges axial with equatorial ligands while route C does not involve such an exchange.

energy structures. Hence the conversion of the regular TBP may stop at the compressed TBP.

(ii) Route B starts with the Berry twist of a regular TBP which is accompanied by a negligible energy loss (0.04 eV). The conversion proceeds further with energy gain. Hence route B is thermally accessible and should be preferred to reach the $C_{2v}$ structure as compared with route A which freezes the regular TBP in the compressed TBP structure.

(iii) Movement along route C is not connected with any energy loss—not in a single stage. It starts with compressing the regular TBP (see Figure 6) and proceeds further with stretching ($\delta S_5$) and bending in the equatorial plane ($\delta S_7$). The order of performing these motions may be reversed, or more likely they should occur concurrently: it is known that when the bonds become shorter, the valence angle formed by these bonds tends to open in order to avoid increased repulsion between the nonbonded atoms.[25] Figure 10 demonstrates this rule in our specific case. Two $C_{2v}$ structures appear in the combined space of $\delta S_5$ and $\delta S_7$. The two structures differ slightly ($\Delta R$ = 0.05 Å, $\Delta\phi$ = 4°, $\Delta E$ = 0.014 eV), structure B being very close to the experimental $C_{2v}$ structure.

If route C is the preferred one, then no Berry twist should be performed on the conversion path. In other words the $\delta S_9$ (axial bending) should be excluded from the distortion mechanism which can be termed as axially pivotal (see ref 21). The different equivalent isotropic thermal parameters $B_{eq}$ for the axial (2.30 Å$^2$) and equatorial (4.40 Å$^2$) Cl atoms in the high-temperature phase, showing a compressed TBP structure,[7] lend support to this claim—after initial axial compression the motion is restricted to the equatorial plane. Moreover, $B_{eq}$ for the axial Cl atoms are close to those for the low temperature $C_{2v}$ structure (1.6 Å$^2$) (see, however, ref 27).

## 5. Conclusions

A very complicated picture is obtained. As expected from the epikernel principle[23] (see also Figure 5) the SP ($C_{4v}$) is a nonstationary point: there is no energy minimum for this structure. It appears as a saddle point connecting two TBPs. The stationary points are with $C_{2v}$ symmetry, but they can be obtained by different mode combinations.

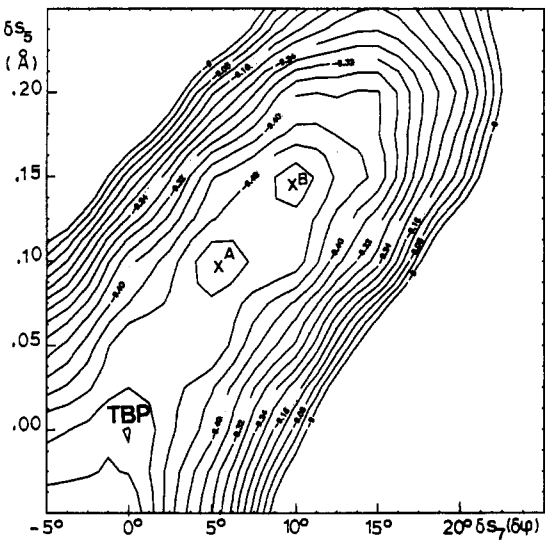


**Figure 10.** Map of the ground-state orbital stabilization vs $\delta S_7$ and $\delta S_5$ modes. The reference structure is a compressed ($R_{ax}$ = 2.3 Å, $R_{eq}$ = 2.4 Å) TBP at $\delta S_7$ = 0 and $\delta S_5$ = 0. The two minima occur at (A) $\delta R$ = 0.1 Å and $\delta\phi$ = 5.5° and (B) $\delta R$ = 0.15 Å, $\delta\phi$ = 9.5°. The energy gain on going from the compressed TBP to structure A is 0.022 eV; that from A to B is 0.0138 eV with 0.0358-eV overall stabilization.

The different symmetry modes of $[CuCl_5]^{3-}$, *taken separately*, produce different shapes when starting with a regular TBP: (i) the two $\alpha_1'$ modes preserve the initial $D_{3h}$ symmetry and they compress the TBP but would not elongate it; (ii) the two bending $\epsilon'$ modes preserve the regular TBP structure with the regular SP ($C_{4v}$) as a saddle point; (iii) the stretching $\epsilon'$ mode reduces the symmetry to $C_{2v}$.

(27) Atanasov, M.; König, W.; Craubner, H.; Reinen, D. *New. J. Chem.* **1993**, *17*, 115.

These results are in full agreement with the epikernel principle.[22] The attempt[11] to modify this principle in the particular case of $[CuCl_5]^{3-}$ should be viewed with caution.

It emerges from this work that the $D_{3h}$–$C_{2v}$ interconversion is a *multimode process*. It involves several symmetry modes which combine in different ways to produce the $D_{3h}$ and $C_{2v}$ structures as static distortion of a parent regular TBP. The participation of the totally symmetric modes, as suggested elsewhere[28] in an out-of-phase combination, is indispensable to promote the conversion mechanism.

The conversion takes place by *multilevel interaction*: it involves mixing of the ground state with *all* states with equal symmetry *produced in the vibrationally displaced symmetry group*.[12] The Cu $d_{x^2-y^2}$ admixing to the new HOMO is crucial.

The two $[CuCl_5]^{3-}$ structures may be related to two separate energy minima that can be reached via different routes: route A to reach the higher-energy compressed TBP $D_{3h}$ structure at the higher temperature and route C to reach the lower energy elongated pyramidal $C_{2v}$ structure at the lower temperature. The choice of route would depend on the available thermal energy.

In view of the complexity of the problem and the inferiority of the semiempirical method employed, the results presented here should be viewed as a broad brush mapping of a possible landscape. It is hoped that they may stimulate others to explore locally with more sophisticated methods. The maps point to the paths that can be followed with some chance of success.

**Acknowledgment.** This work was partially supported by Grant No. 136 of the Bulgarian National Research Fund. The author is grateful to the reviewers, whose critical remarks helped improve the text.

(28) Ballhausen, C. J. *Coord. Chem. Rev.* **1990**, *100*, 29.

## Appendix

The four sets of parameters shown in Table 5 were used in the calculations.

**Table 5**[a]

| | set I | set II | set III |
|---|---|---|---|
| Cu | | | |
| $\zeta$ (3d) | 6.684(0.486) | 5.95(0.5933) | 5.95(0.6062) |
| | 2.777(0.657) | 2.30(0.5744) | 2.50(0.5371) |
| $\zeta$ (4s) | 2.200 | 2.05 | 2.05 |
| $\zeta$ (4p) | 2.200 | 1.325 | 1.325 |
| IP(3d) | −14.00 | −20.81 | −13.64 |
| IP(4s) | −11.40 | −15.44 | −10.16 |
| IP(4p) | −6.06 | −9.393 | −4.96 |
| Cl | | | |
| $\zeta$(3s) | 2.183 | 2.033 | 2.033 |
| $\zeta$(3p) | 1.733 | 2.033 | 2.033 |
| $\zeta$(3d) | | 2.033 | |
| IP(3s) | −36.3 | −30.00 | −22.88 |
| IP(3p) | −14.2 | −15.00 | −14.21 |
| IP(3d) | | −9.00 | |
| k | 2.00 | 1.78 | 2.00[b] |

[a] Ionization potentials IP are in eV. [b] Geometric mean.

Set I was taken from Calzaferri's collection,[15] set II was used in ref 16 and coincides in general with the parameters in the original ICON program (QCPE No. 545), and set III was that of Hatfield et al.[17]